

The Physics of Macropore Formation in Low-Doped p-Type Silicon

V. Lehmann^{a,*} and S. Rönnebeck^b

^aSiemens AG, 81730 Munich, Germany

^bFaculty of Engineering, University of Kiel, 24143 Kiel, Germany

The dependence of the morphology of macropores in p-type silicon electrodes on formation parameters such as substrate doping density, electrolyte composition, and applied current density is investigated. The results are compared with the well-understood case of electrochemical macropore formation on n-type silicon electrodes. A growth model is derived in which pore formation is shown to be a consequence of charge-transfer mechanisms in a Schottky diode applied to a nonplanar interface.
© 1999 The Electrochemical Society. S0013-4651(98)11-103-5. All rights reserved.

Manuscript submitted November 23, 1998; revised manuscript received March 5, 1999.

The electrochemical formation of porous silicon (PS) on silicon electrodes anodized in HF has been known for four decades.¹ The structural dimensions of these PS films are very small and mostly microporous. The first report of the formation of large macropores on p-type silicon electrodes was published only 4 years ago.² This late discovery was first ascribed to the fact that water-free mixtures of pure HF and an organic solvent were used for anodization,^{2,3} while porous silicon has been formed only in HF electrolytes containing a certain fraction of water, so far. Later investigations, however, showed that in organic electrolytes with some water⁴ or even in pure aqueous solutions of HF^{5,6} macropore formation on p-type substrates can be observed.

Macropore formation on n-type substrates in aqueous HF was first observed in 1972⁷ and studied in detail in the 1990s.^{8,9} On n-type substrates the active state of the pore tips is due to their collection efficiency for minority charge carriers (holes), which are required to initiate the dissolution process. The passivation of the pore walls is ascribed to a depletion of holes in the walls between the pores.

Macropore formation in p-type silicon is surprising on first sight because, in contrast to n-type silicon, p-type electrodes are under forward conditions. An extended space-charge region (SCR) is therefore not expected for a p-type electrode in the anodic regime. Consequently most models for macropore formation on p-type Si electrodes are based on passivation effects, other than the SCR. The absorption of organic molecules on the electrode, for example, is proposed to change locally the rate of silicon dissolution.⁴ Another model explains macropore formation by electrostatic considerations: if the resistivity of the silicon electrode is higher than that of the electrolyte, every perturbation on the interface is enhanced by accumulated field lines. In contrast to the case of n-type silicon, the passivation is proposed to be due to the resistivity of the silicon substrate material and not due to a space-charge region.^{5,6} However, both models are found to be in contradiction with experimental observations. The prior model is put in question because macropores form on p-type electrodes in electrolytes free of organic compounds,⁵ while the latter model is questionable because macropore formation is observed in electrolytes with a resistivity more than two orders of magnitude larger than that of the silicon substrate.⁴

In this report new experimental data of macropores formed in p-type Si electrodes of different doping densities by anodization in HF under various conditions are presented. These results are compared with data obtained for n-type electrodes under similar conditions. The investigation aims at a pore-formation model which is in accordance with the experimental observations.

In order to use a consistent terminology, the word "hole" always refers to a defect electron, while a pore is understood as an etch pit whose depth exceeds its width.

Experimental

Polished silicon substrates of {100} and {110} crystal orientation and of various doping densities were used for the experiments. In order to study the pore initiation process, some substrates were prepatterned with arrays of alkaline etch pits. An ohmic contact to the Si electrode was realized by rubbing GaIn eutectic on the back side. Anodization of p-type substrates was performed under galvanostatic conditions in a simple O-ring cell in the dark, with a Pt wire as counter electrode. Back side illumination was used to generate the required holes for dissolution in n-type Si electrodes.⁸ All electrolytes were prepared from very large scale integration (VLSI) grade aqueous HF (50%). Optical microscopy was found to be sufficient to study the macropore morphology. The dissolution valence was determined gravimetrically using a scale with 1 μg resolution.

Results and Discussion

In a preliminary experiment, the results of Ponomarev and co-workers⁴ were reproduced using 2 M HF in acetonitrile (prepared from 68 mL of 50% HF and 932 mL acetonitrile) as an electrolyte. A cross-sectional micrograph of the resulting porous structure is shown in Fig. 1a. The resistivity of the as-prepared electrolyte was determined to be about 5000 $\Omega\text{ cm}$, which is more than two orders of magnitude larger than the resistivity of the p-type Si electrode (20 $\Omega\text{ cm}$). This result is in contradiction to the electrostatic model of Wehrspohn *et al.*,^{5,6} which states that pore formation can be observed only for electrode resistivities higher than or equal to the electrolyte resistivity.

Based on their results, Ponomarev and co-workers⁴ concluded that a passivation by absorption of organic molecules is responsible for macropore formation. In order to test this model, pure aqueous HF was used as an electrolyte. The result is shown in Fig. 1b and c (30% HF, 20 $\Omega\text{ cm}$, 40 mA/cm², 7.5 min, room temperature). Macropore formation is clearly observed in pure aqueous solutions of HF. The change in pore morphology in the micrograph (right to left in Fig. 1b) is probably due to inhomogeneities in doping. Such inhomogeneities originate from the crystal growth process and are known as striations. A (scanning electron microscope) SEM micrograph of this sample, shown in Fig. 1c, reveals that most of the pore volume is filled with microporous Si. From the result shown in Fig. 1b and c, it can be concluded that organic solvents play no major role in the dissolution reaction that is connected with macropore formation. Consequently all following experiments were performed in aqueous HF. In order to develop a consistent model of macropore formation in p-type silicon, the effect of the different formation parameters needs to be investigated in detail.

In a set of anodization experiments the effect of doping density on macropore morphology was investigated. The resulting morphology was not inspected by cleaving the sample but by polishing it under a small angle of about 10° to the surface. This enabled us to study the change of pore cross section with depth. Figure 2a-d shows

* Electrochemical Society Active Member.

micrographs of p-type substrates of different doping, anodized under identical conditions in the dark (10% HF, 3 mA/cm², 90 min, room temperature). It can be seen that pore diameter, as well as pore wall thickness, decrease with decreasing p-type substrate resistivity. The pore wall thickness w is always found to be smaller than the pore

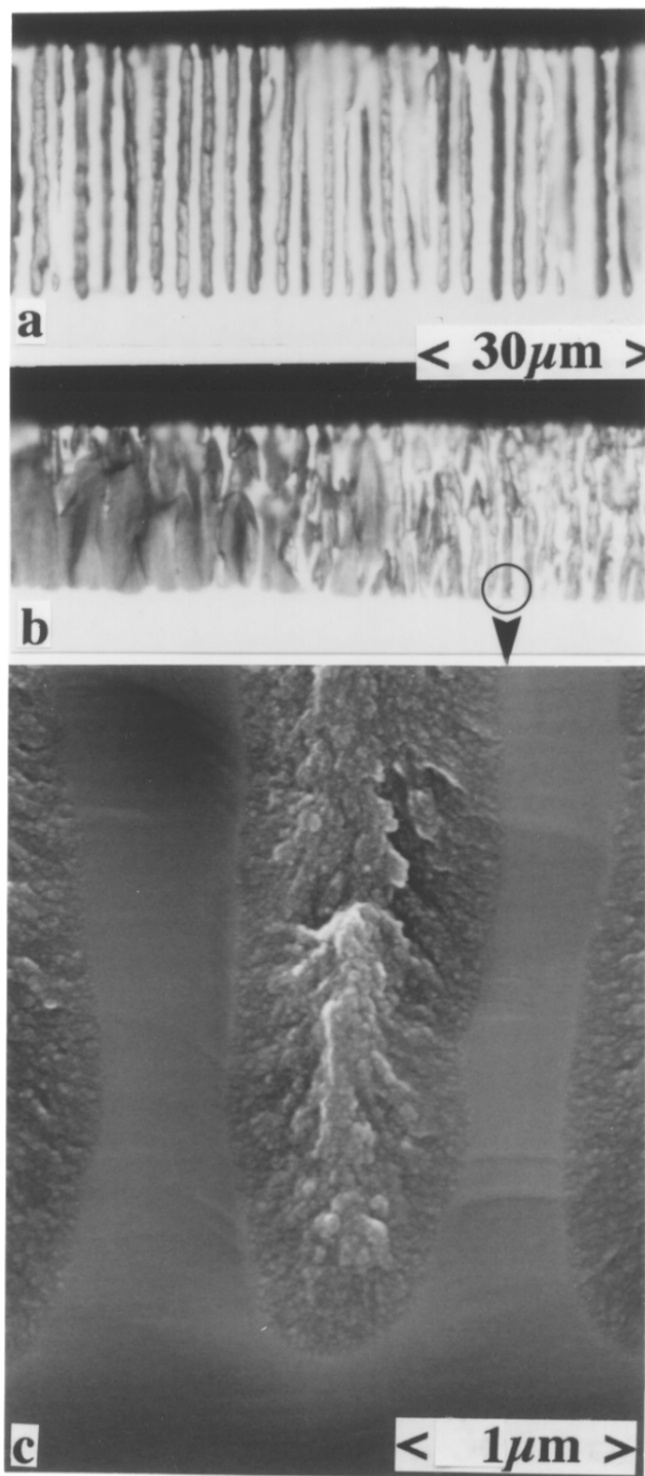


Figure 1. Cross-sectional optical micrographs of macropores formed on p-type silicon electrodes by anodization in (a) a mixture of HF and an organic solvent (2 M HF, 20 Ω cm, 3 mA/cm², 90 min, {100}, room temperature) and (b) in aqueous HF (30% HF, 20 Ω cm, 40 mA/cm², 7.5 min, {100}, room temperature). (c) A SEM micrograph of sample (b) reveals that most of the pore volume is filled with microporous silicon.

diameter. If the pore wall thicknesses from Fig. 2a-d are plotted vs. the substrate doping density, a square root dependence is observed, as shown in Fig. 3.

In order to compare these results with macropore formation on n-type Si, an n-type sample was etched under strong back side illumination and low bias (10% HF, 3 mA/cm², 30 min, room temperature, 0.2 V). Note that under these conditions the current density is not limited by illumination but by applied bias. The resulting morphology is shown in Fig. 2e. The macropore diameters are found to be comparable to the p-type case, while the pore spacing is much wider on the n-type substrates. The pore growth rate is larger by a factor of about three on the n-type substrate. A plot of the average pore density vs. doping density for random macropore formation on polished p-type and n-type electrodes is shown in Fig. 4. The regime for stable macropore array fabrication on n-type substrates (shaded region) is shown, too. For n-type as well as p-type Si, the dependence of pore density on doping density is roughly linear; only for very low doped samples is a significant deviation from this law observed.

If the p-type substrate resistivity is reduced to 5 Ω cm, the walls of the macropores become very thin and are too fragile for polishing; a cleaved sample is shown in Fig. 5b (5 Ω cm, 10% HF, 3 mA/cm², 90 min, room temperature). For substrate resistivities below 5 Ω cm, only a roughening of the electrode surface was observed (2 Ω cm, 10% HF, 3 mA/cm², 90 min, room temperature). In order to investigate whether this lower resistivity limit for macropore formation is sensitive to variations of electrolyte resistivity, anodization was performed in HF of different concentrations. As shown in Fig. 5a-c, neither increase nor decrease of the concentration of the aqueous HF was sufficient to produce more stable pore walls than for the case of 10% HF.

Next the effect of current density on macropore formation was investigated. Figure 6a-c shows micrographs of polished (top) and cleaved (bottom) p-type electrodes anodized at various current densities (50 Ω cm, 10% HF, 90 min, room temperature). It is observed that the pore depth is roughly proportional to the current density for a constant anodization time. This is in stark contrast to stable macropore formation on n-type substrates, where the pore depth is independent of applied current density.⁸ The upper part of Fig. 6 shows thinner pore walls and a tendency to faceting along {110} planes for higher current densities. The porosity increases slightly with current density. Due to dying of pores, the pore diameter is somewhat larger in the pore tip region. Note that only in Fig. 6a (top) the whole polished porous region is shown; Fig. 6b and c (top) show only the polished pore tip region. Close to the initial electrode surface (not shown in Fig. 6b and c) the pore diameters are observed to be equal, independent of applied current density. The increase in pore diameter from left to right in Fig. 6a is therefore due only to a reduction of pore density with increasing pore depth. Macropore formation on p-type substrates was never observed for current densities close to, or above, the critical current density J_{PS} . At low HF concentrations, macropores are found to disappear already at about $J_{PS}/10$, as shown in Fig. 7a-c (20 Ω cm, 3% HF, 16.2 As/cm², room temperature).

The macropore growth rate is calculated by dividing the pore depth as shown by the micrographs by the anodization time. The observed values are a factor of 1 to 1.5 larger than the growth rates for microporous silicon. Their increase with current density, however, is similar to that for micro- and mesoporous silicon, as shown in Fig. 8. This is in contrast to the growth rate of n-type macropores, which is virtually independent of current density.

The dissolution valence n , the number of charge carriers required for the dissolution of a Si atom, was determined gravimetrically. The observed values are close to the ones observed for microporous silicon formation, as shown in Fig. 9. The decrease of n for macropore formation below the values observed for micropore formation is an artifact, due to the fact that the total etch time for the macropore samples was about three times the etch time for the microporous reference. Consequently the pure chemical etching of the microporous film in the macropores produced a larger decrease of n than for the microporous samples. The values for n observed for high current densities are more

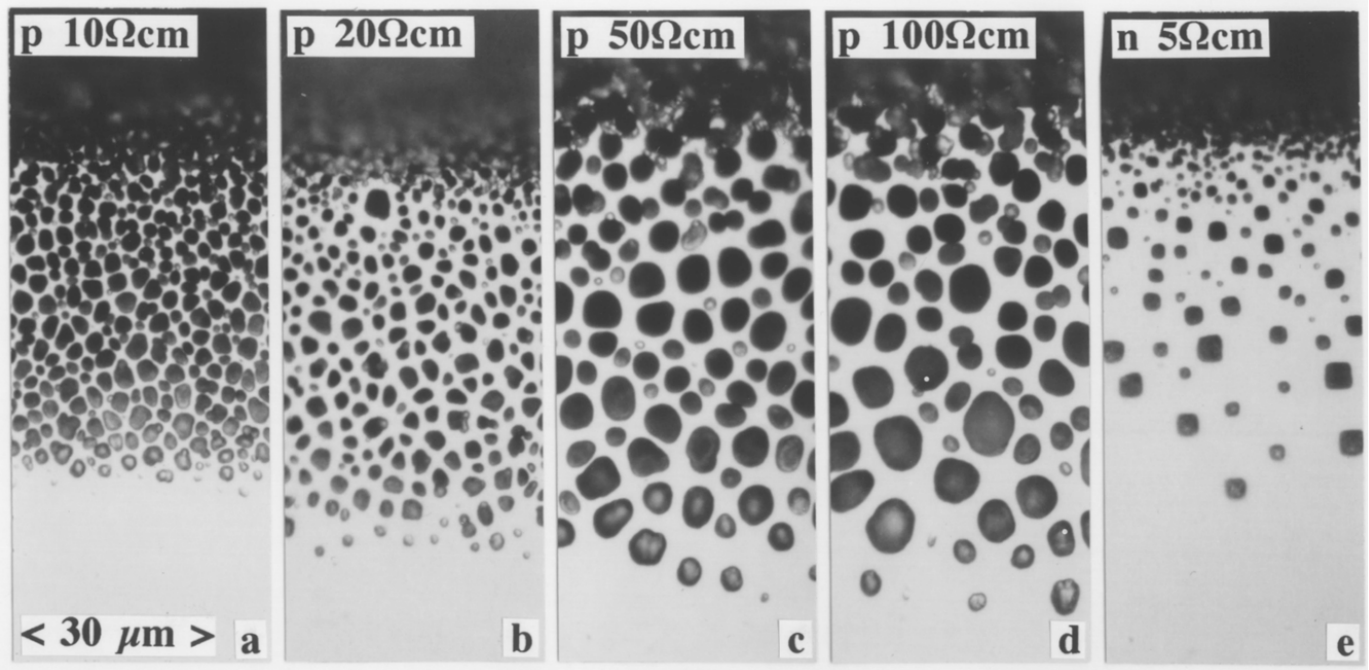


Figure 2. (a-d) Optical micrographs of p-type substrates of different doping densities polished under a small angle, after anodization under identical conditions in the dark (10% HF, 3 mA/cm², 90 min, {100}, room temperature). (e) An n-type substrate anodized under similar conditions is shown for comparison (10% HF, 5 Ω cm, 3 mA/cm², 30 min, 0.2 V, {100}, room temperature).

reliable because the electrochemical etching time, measured in minutes, is short enough to neglect pure chemical etching.

The dependence of p-type macropore morphology on the crystal orientation of the substrate was investigated by anodization of {110} oriented Si electrodes. Results are shown in Fig. 10. The pores show a tendency to branch at low current densities (Fig. 10a), while for an increased current density branching is reduced and the pores grow more perpendicular to the surface (Fig. 10b). For n-type substrates the <100> direction of pore growth is maintained even at higher current densities (Fig. 10c).¹²

Macropore growth on n-type substrates can be initiated by etch pits. Such etch pits can, for example, be generated by photolitho-

graphic patterning of an oxide or nitride film and subsequent alkaline etching.^{8,9} As shown in Fig. 11b-d (50 Ω cm, 3% HF, 2 mA/cm², room temperature), the same technique is found to work for macropores on p-type Si electrodes if the pore spacing of the pattern is close to the random pore density according to Fig. 4. However, further growth of p-type macropores is found to be not as stable concerning pore depth and growth direction as for the case of n-type substrates.

Formation Model

A silicon electrode anodized in HF is under depletion in the regime of porous silicon formation and behaves therefore like a

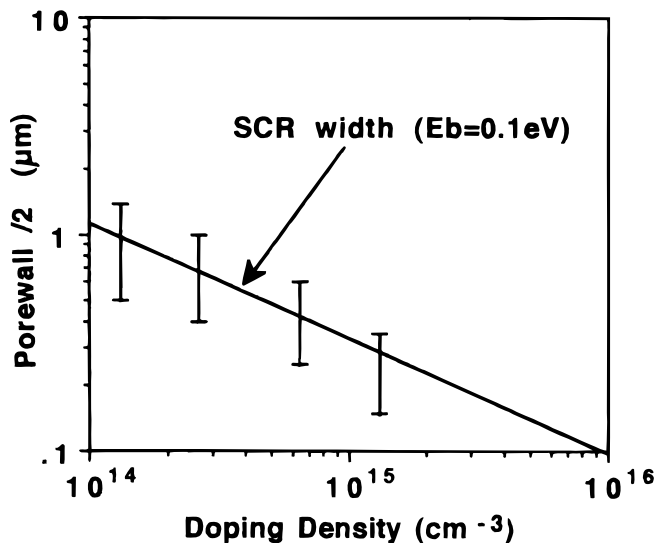


Figure 3. Values of pore wall thickness from Fig. 2a-d as a function of doping density (error bars) together with the space-charge region width for a potential ($V_{bi} + V - 2kT/e$) of 0.1 V (line).

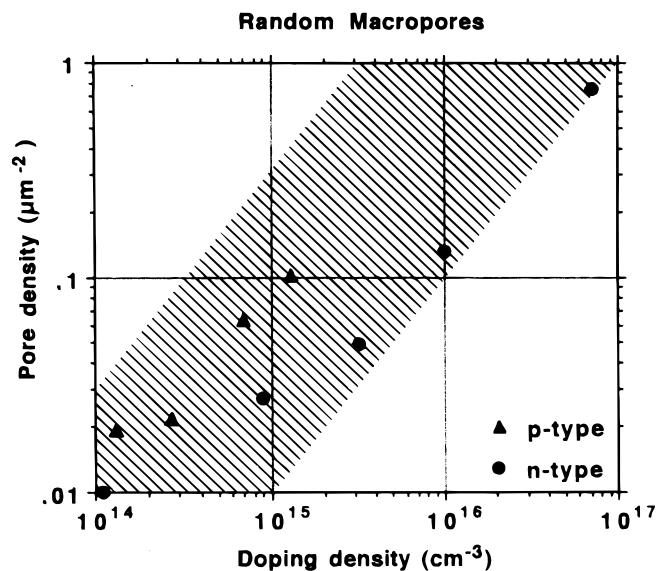


Figure 4. Values of macropore density observed for random pore formation on polished n-type (circles), as well as p-type substrates (triangles) as a function of Si substrates doping density. The regime of stable formation of macropore arrays on n-type Si is shown too (dashed area).

solid-state Schottky diode.¹⁰ We now show that macropore formation on p-type substrates can be understood as a consequence of the charge-transfer mechanisms in a Schottky diode if applied to a non-planar interface.

The basic electrostatics of the porous electrode is sketched in Fig. 12. No electric field is present in the bulk electrode. Neutrality requires the hole concentration n_h to be equal to the acceptor concentration N_A , there. Close to the interface with the electrolyte a space-charge region (SCR) is present in the semiconductor electrode. The width W of the space-charge region depends on the built-in potential V_{bi} , on the p-type doping density, on the applied bias V_{app} , and on the interface geometry. The latter factor is a key to the understanding of pore formation and is discussed in some detail. By solving the Poisson equation, W can be calculated for different geometries. With a doping density of $N_A = 10^{15} \text{ cm}^{-3}$ and a potential $V = (V_{bi} - V_{app}) - 2kT/e$ of 0.5 V, W is 785 nm for the planar case. At the walls of a cylindrical pore of the radius $r = 500 \text{ nm}$, W is reduced to 680 nm, due to geometrical field enhancement. At a hemispherical pore tip of radius $r = 500 \text{ nm}$, W is further reduced to 590 nm. W becomes even smaller for conical pore tips. In conclusion, W becomes minimal at the pore tip, while the barrier height $E_b = e(V_{bi} - V_{app}) - 2kT$ is independent of geometry.

After electrostatics, charge-transfer is the next topic. A p-type silicon electrode anodized in HF behaves very similarly to a solid-state Schottky diode under forward conditions. The forward current of a Schottky diode is either dominated by diffusion, by thermionic emission, or by tunneling of holes.

At zero bias and under forward conditions, the SCR is not fully depleted of holes. Consequently a diffusion current I_{diff} exists which is due to the concentration gradient of holes dn_h/dr , according to the Schottky theory. At thermal equilibrium and for zero applied bias, I_{diff} is compensated by the field current I_{field} . This is true for the pore walls as well as for the pore tip. The absolute values of I_{diff} and I_{field} , however, are larger at the pore tip, because the concentration gradient dn_h/dr , as well as the electric field strength, increases with decreasing W , as sketched in the left part of Fig. 13. If a forward bias V_{app} is applied I_{field} decreases, while I_{diff} increases. Now the higher absolute current density values at the tip become decisive. The total

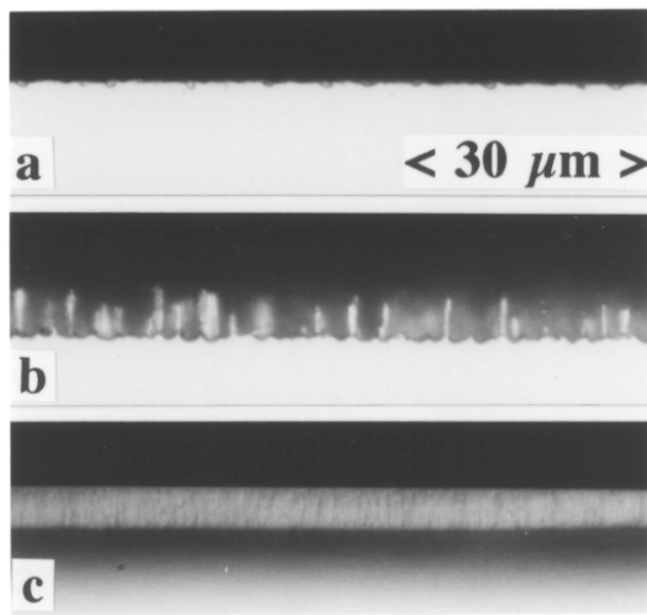


Figure 5. Macropore formation on p-type Si as a function of aqueous HF concentration (5 Ω cm, 3 mA/cm², 90 min, {100}, room temperature). (a) Only an increase of surface roughness is observed for 3% HF. (b) Macropores with fragile walls are formed in 10% HF. (c) Only a microporous Si layer is observed in 30% HF.

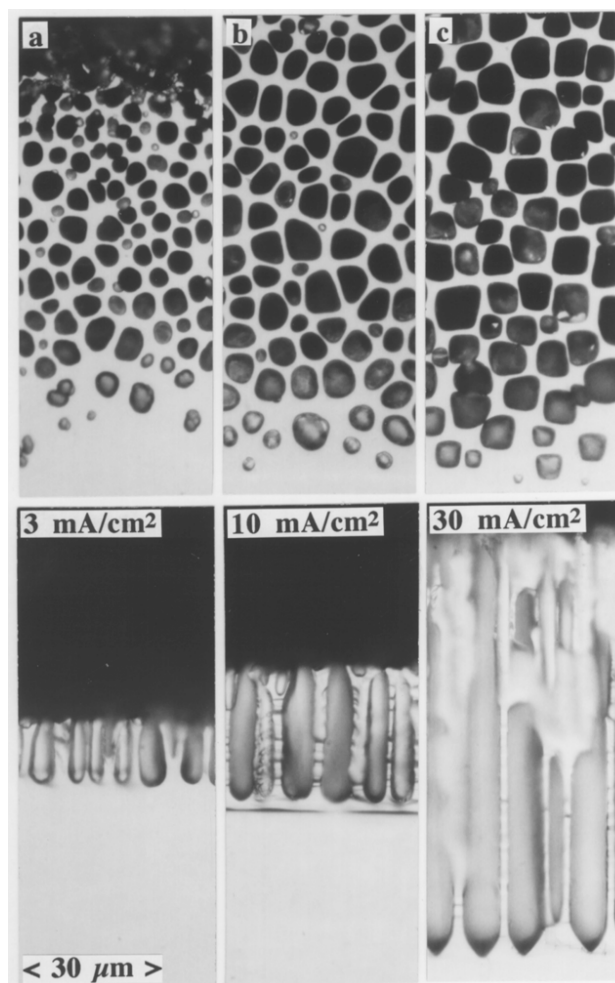


Figure 6. Macropore formation on p-type Si as a function of applied current density (50 Ω cm, 10% HF, 90 min, {100}, room temperature), cross sections (bottom), and samples polished under a small angle (top). A linear increase of pore depth with current density is observed (a) 3, (b) 10, and (c) 30 mA/cm².

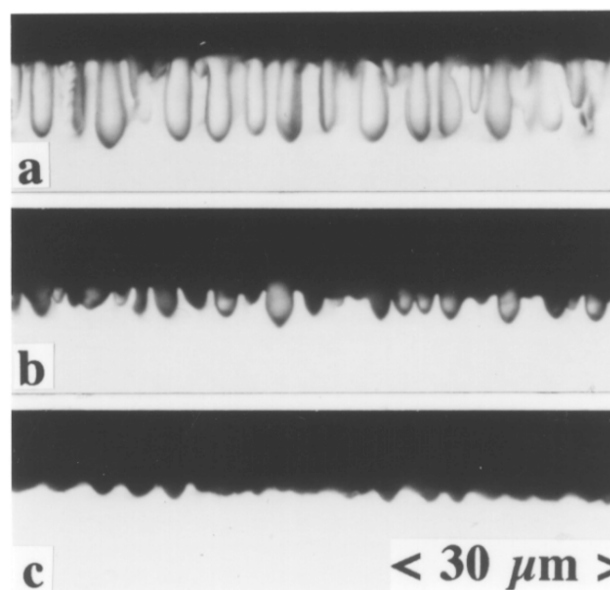


Figure 7. At low HF concentrations macropore formation on p-type Si is found to be suppressed for an increase of applied current density above a certain value (20 Ω cm, 3% HF, 16.2 As/cm², {100}, room temperature). (a) 2, (b) 3, and (c) 4.5 mA/cm².

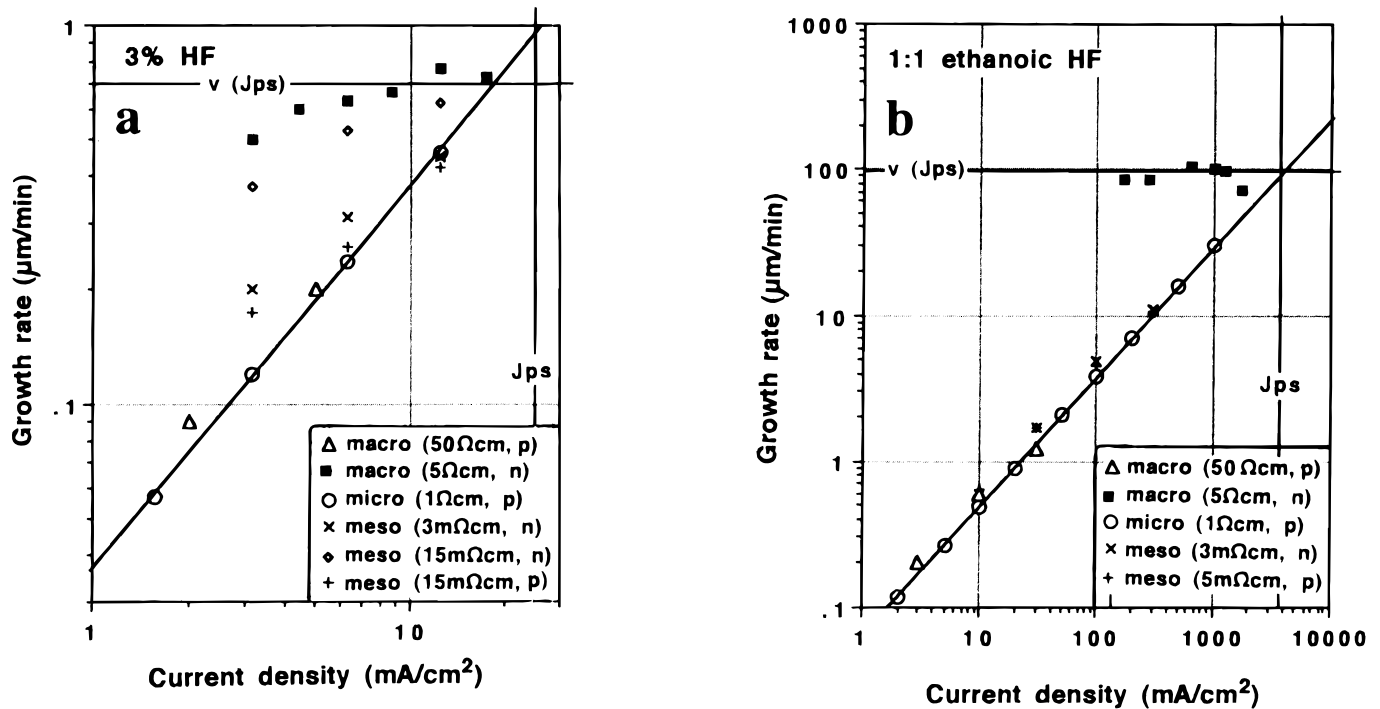


Figure 8. Pore growth rates in (a) 3% aqueous HF and (b) ethanoic HF for different substrate doping kinds and densities as indicated in the figure. Note that high growth rates are observed for low and moderately doped n-type substrates.

current density at the tip $I_{tip} = (I_{diff} - I_{field})_{tip}$ is always larger than the current density at the wall $I_{wall} = (I_{diff} - I_{field})_{wall}$. As a consequence a depression in the electrode surface grows faster than a planar area: a pore tip develops. If the distance between two neighboring pores becomes smaller than $2W$ the pore wall becomes passivated due to the depletion of holes in the SCR.

After diffusion, the effect of thermionic emission over the barrier on pore formation is the next topic. The theory for this kind of charge transfer has been developed by Bethe. The thermionic emission current I_{therm} is due to holes that have sufficient energy to overcome the potential barrier and are traversing in the r direction. However, a significant contribution of this kind of transport can be ex-

pected only if the main free path of such holes exceeds the SCR width W . The SCR width during macropore formation can be approximated from the results of Fig. 2 under the assumption that the

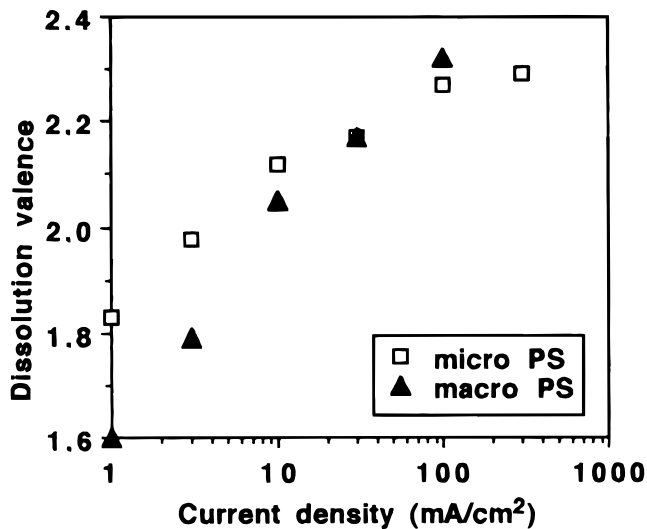


Figure 9. Dissolution valence n as a function of applied current density in ethanoic HF, for macropore formation on $50 \Omega \text{ cm}$ p-type electrodes (solid triangles). For comparison n is also shown for the formation of microporous Si on $1 \Omega \text{ cm}$ p-type electrodes (open squares).

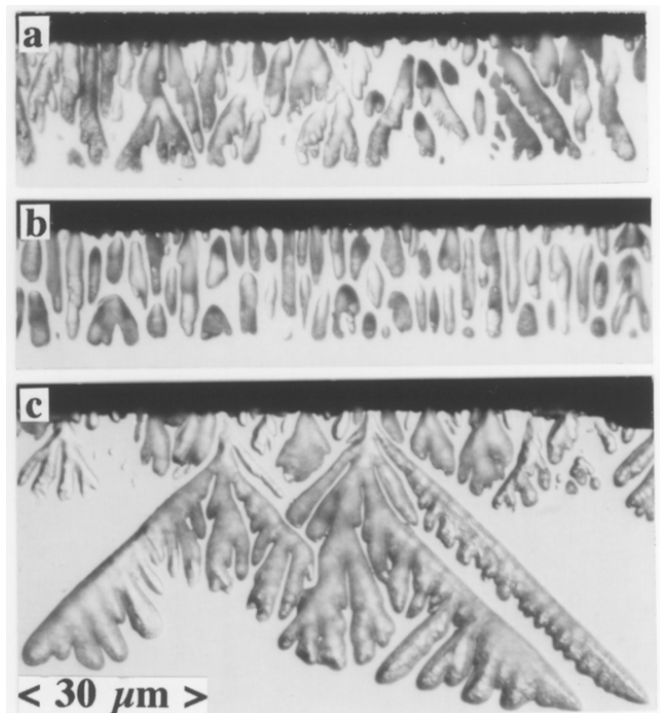


Figure 10. Optical micrographs showing the polished $\{100\}$ plane of $\{110\}$ oriented substrates after macropore formation. The orientation dependence is less pronounced for p-type substrates (a) 1 mA/cm^2 , 400 min and (b) 2 mA/cm^2 , 200 min (10% HF, $15 \Omega \text{ cm}$, room temperature), if compared to an n-type substrate (c) (4% HF, $3 \Omega \text{ cm}$, 4 mA/cm^2 , 143 min, 1.5 V, room temperature).

pore walls are depleted if their thickness is $2W$. Figure 3 shows a square root dependence of W on N_A , this enables us to approximate a barrier height E_b present during macropore formation. A barrier height of $E_b = 0.1$ eV is approximated from Fig. 3, which corresponds well with values of E_b resulting from impedance measurements.¹⁰ The velocity of holes in a semiconductor shows a thermal distribution around kT , the high energy tail of this distribution contains holes with sufficient energy to cross the barrier ($E_b = 0.1$ eV). The main free path p of holes can be calculated from their velocity v and from the mean free time τ between two collisions with phonons. The time τ is calculated using the hole mobility $\mu_h = 500$ cm²/V s, the mean effective hole mass $m_h = 0.33 m_e$ (m_e = rest mass of electron), and the elementary charge e , by $\tau = \mu_h m_h / e$, to be $\tau = 10^{-13}$ s. Using $E_b = 1/2 m_h v^2$, a velocity $v = 3.3 \cdot 10^5$ m/s is obtained for a barrier height of 0.1 eV. This gives the mean free path p to be about $p = 33$ nm. This mean free path corresponds to the SCR width present in a p-type substrate of $N_A = 10^{17}$ cm⁻³ (corresponding to 0.2 Ω cm) for a barrier height of 0.1 eV. In conclusion, for p-type substrate doping densities above 10^{17} cm⁻³, thermionic emission is assumed to dominate the charge transfer. Thermionic emission is sensitive to the barrier height E_b but not to the barrier

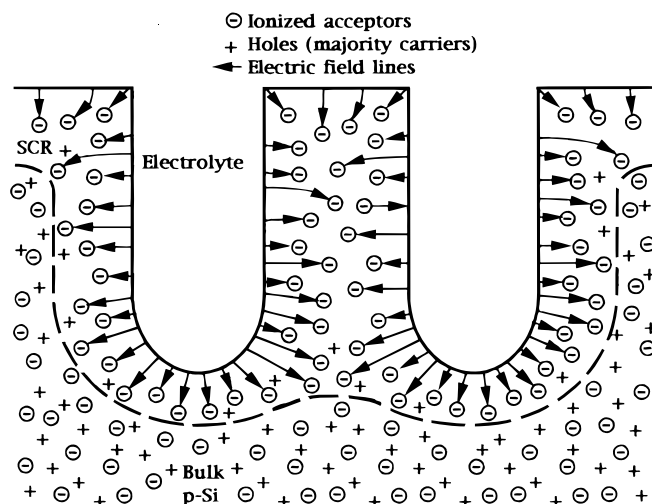


Figure 12. Sketch of the equilibrium charge distribution and the electric field around pores in a p-type semiconductor electrode.

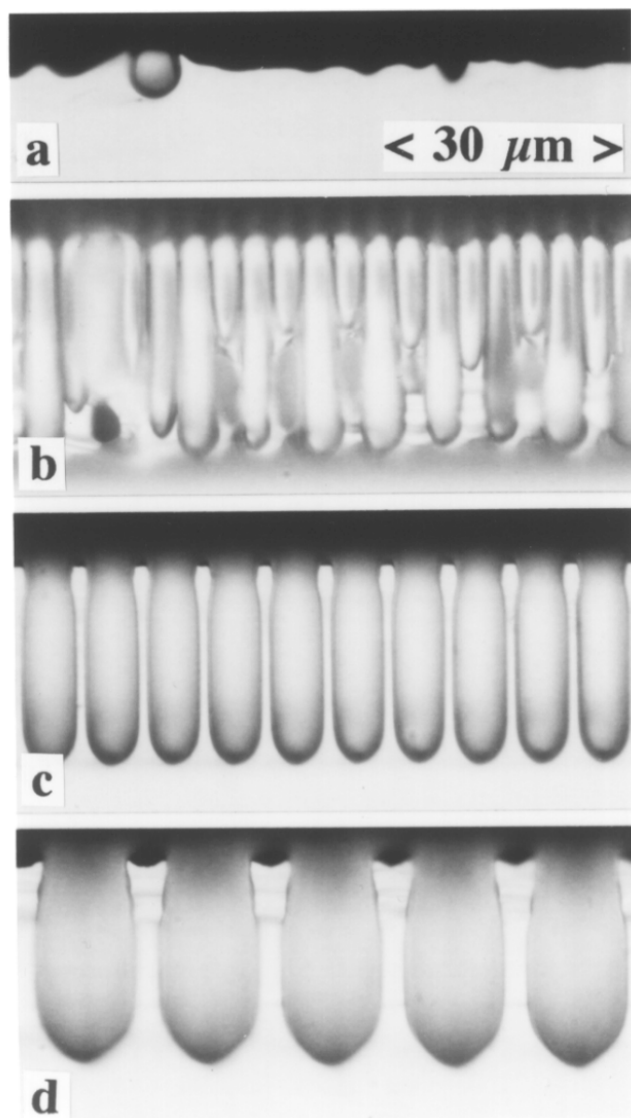


Figure 11. (a) Macropore formation on a planar p-type Si electrode and (b) on p-type Si electrodes prepatterned by alkaline etch pits of different pitch (b) 4, (c) 8, and (d) 16 μ m pitch (50 Ω cm, 3% HF, 2mA/cm² 240 min, {100}, room temperature).

width W , if the latter is smaller than the mean free path. Consequently depressions show no higher current density than planar sections: no pores form. The calculated upper doping limit for pore formation (10^{17} cm⁻³) is about one order of magnitude larger than the experimentally observed value (10^{16} cm⁻³). However, several approximations, which may contain significant error, have been used in the calculations. In addition it is not known at which thermionic contribution to the total current pore formation is suppressed.

The third charge-transfer mechanism is not relevant to macropore formation, however, it is discussed to give the full picture. Tunneling of charge carriers becomes the dominant transfer process at doping densities of $N_A = 10^{18}$ cm⁻³ (corresponding to 0.045 Ω cm p-type) at room temperature. Similar to the diffusion current, the tunneling current is sensitive to the barrier width. This again leads to pore formation, however the dimension of the SCR are now measured in nanometers rather than micrometers. Consequently mesoporous layers are expected. This is supported by experimental observations which show that, for doping densities between 10^{18} and 10^{19} cm⁻³, purely mesoporous layers are formed on p-type silicon electrodes. Only for very high p-type doping densities (10^{20} cm⁻³) are larger pore diameters reported.¹¹ The formation mechanism and the morphology of mesoporous layers on silicon electrodes will be discussed in detail in a forthcoming paper.¹³

In conclusion macropore formation on p-type silicon electrodes in HF is due to the increase of the diffusion current density at pore

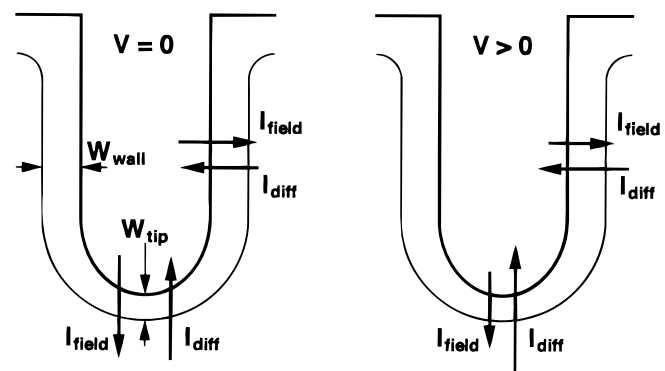


Figure 13. (a, left) Equilibrium ($V=0$) field currents and diffusion currents across the space-charge region for the macropore tip and wall region in p-type Si. (b, right) Field currents and diffusion currents under forward bias ($V>0$). Note that due to geometric field enhancement around the pore tip the tip currents are always larger than the pore wall currents.

tips, compared to flat electrode areas. The origin of this increase is the pore tip geometry, which produces a minimum of SCR width at the tip and consequently a maximum hole concentration gradient. Pore walls become passivated against dissolution if their distance decreases to two times the SCR width, because holes which initiate the dissolution process become depleted. Pore formation is suppressed if the charge transfer becomes dominated by the thermionic emission process, which is sensitive only to barrier height and not to barrier width.

Comparison with macropore formation on n-type electrodes.—In contrast to p-type electrodes, an n-type electrode is under reverse conditions in the anodic regime. This has several consequences for pore formation.

The dissolution process of an n-type Si electrode under reverse conditions is due to minority carriers (holes). The concentration of minorities is very low under equilibrium conditions. Illumination, for example, is required to increase their concentration. Now three kinds of charge carriers are present in the electrode: ionized dopants, electrons (majority charge carriers), and holes (minority charge carriers). Concentration gradients of holes in the bulk semiconductor may exist now, because their charge is compensated by the electron distribution which establishes neutrality in the bulk. As a conse-

quence the strict requirement for p-type macropores that the wall thickness w needs to be smaller than $2W$ for passivation does not apply for n-type substrates anymore. This is visualized by macropores grown in the stable pore formation regime using patterns of different pitch, as shown in Fig. 14. Even if the pores are separated by much more than $2W$, the hole concentration (indicated by dots in Fig. 14) is close to zero between the pore walls due to their diffusional distribution. The distance between two n-type macropores required for passivation is therefore limited by the minority-carrier diffusion length rather than by the SCR width.

Another difference from the p-type case concerns the pore tip condition. The reverse bias, for stable macropore formation on n-type substrates, has to be larger than the bias V_{PS} corresponding to the critical current density J_{PS} .⁹ The pore-tip current density is therefore not limited by bias. The pore tips collect holes until J_{PS} is reached at the tip. A further increase to values larger than J_{PS} would correspond to electropolishing and is therefore not consistent with pore formation. J_{PS} is a function of the HF concentration and the temperature only. As a consequence the growth rate of n-type macropores is independent of applied current density.

On p-type substrates, the applied bias determines the pore-tip current density. It has to be significantly lower than V_{PS} for pore formation. Consequently the pore-tip current density on a p-type sub-

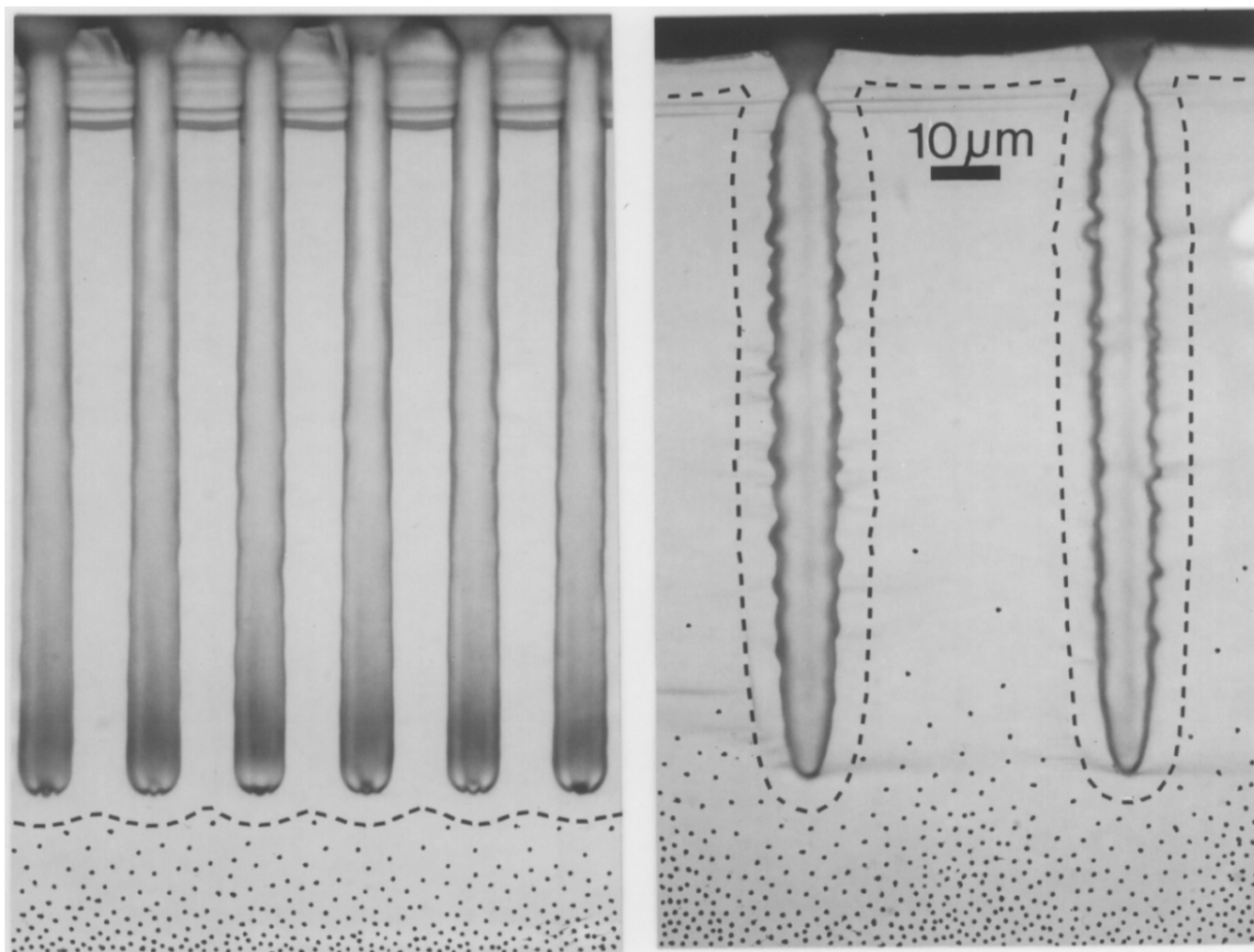


Figure 14. Macropore formation on prepatterned n-type Si electrodes ($40 \Omega \text{ cm}$, 4% HF, 143 min, 2 V, $\{100\}$, 15°C) using (a, left) $8 \times 8 \mu\text{m}$ pitch (5 mA/cm^2) and (b, right) $8 \times 48 \mu\text{m}$ pitch (1.6 mA/cm^2). The minority carrier concentration (dots) and the SCR width (dashed line) are sketched as well. Note that for both cases the pore walls are depleted of holes.

strate is always smaller than J_{PS} . This condition together with the strict requirement for pore-wall passivation ($w < 2W$) produces a growth rate roughly proportional to the applied current density.

Conclusions

The experimental observations of macropore formation in p-type Si electrodes are summarized in points 1-9 below.

1. An organic component in the electrolyte is not required for macropore formation on p-type substrates. Macropore formation is observed for substrate resistivities above 5 Ω cm in aqueous hydrofluoric acid of various concentrations. For lower resistivities only an increase of surface roughness is observed.

2. The average pore-wall thickness observed for random macropore formation on p-type Si corresponds to two times the space-charge region width for an energy barrier of about 0.1 eV.

3. The porosity of random as well as ordered macropore structures is usually high (>50%) and shows only a weak dependence on current density.

4. The dissolution valence is found to be close to that of microporous silicon formation.

5. The macropore growth velocity v increases significantly with applied current density and is equal to or slightly larger than the one observed for microporous silicon formation. The macropore growth velocity increases with increasing HF concentration for a constant applied current density.

6. The pore diameter of random arrays increases with decreasing doping density. It shows no significant dependence on current density.

7. Pore tips and walls are covered with micro-PS. For high HF concentrations, most of the pore volume is filled with micro-PS.

8. Macropores formed on p-type substrates grow preferably in the $\langle 100 \rangle$ direction; however, the dependence on crystal orientation is weaker than for macropore formation on n-type substrates.

9. Etch pits are sufficient to initiate the growth of macropores on p-type substrates.

Points 2 through 8 are in some respect consequences of the fact that depletion in p-type substrates is present only for an applied bias

lower than the one corresponding to the critical current density J_{PS} . Consequently J_{PS} can never be reached at the pore tip, which is in stark contrast to the case of stable macropore formation on n-type substrates.

A model for macropore formation on p-type electrodes is derived based on the charge-transfer mechanisms across the Schottky barrier. The barrier width is reduced at depressions and pore tips due to their geometry. This leads to local increases of the diffusion current, which dominates charge transfer at low doping densities. A depletion of holes passivates the pore walls if they are smaller than two times the barrier width. For moderate p-type doping, thermionic emission over the barrier becomes dominant. This process is not sensitive to barrier width; consequently pore formation is suppressed. At high p-type doping, tunneling dominates, which is again sensitive to barrier width. As a consequence, mesopore formation is observed in this doping regime.

Siemens AG assisted in meeting the publication costs of this article.

References

1. D. R. Turner, *J. Electrochem. Soc.*, **105**, 402 (1958).
2. E. K. Probst and P. A. Kohl, *J. Electrochem. Soc.*, **141**, 1006 (1994).
3. M. M. Rieger and P. A. Kohl, *J. Electrochem. Soc.*, **142**, 1490 (1995).
4. E. A. Ponomarev and C. Levy-Clement, *Electrochem. Solid-State Lett.*, **1**, 42, (1998).
5. R. B. Wehrspohn, J.-N. Chazalviel, F. Ozanam, and I. Solomon, *Thin Solid Films*, **297**, 5 (1997).
6. R. B. Wehrspohn, J.-N. Chazalviel, and F. Ozanam, *J. Electrochem. Soc.*, **145**, 2958 (1998).
7. M. J. J. Theunissen, *J. Electrochem. Soc.*, **119**, 351 (1972).
8. V. Lehmann, *J. Electrochem. Soc.*, **140**, 2836 (1993).
9. V. Lehmann and U. Gruning, *Thin Solid Films*, **297**, 13 (1997).
10. I. Ronga, A. Bsiesy, F. Gaspard, R. Herino, M. Ligeon, and F. Muller, *J. Electrochem. Soc.*, **138**, 1403 (1991).
11. A. Janshoff, K.-D. S. Dancil, C. Steinem, D. P. Greiner, V. S.-Y. Lin, C. Gurtner, K. Motesharei, M. J. Sailor, and M. R. J. Ghadiri, *J. Am. Chem. Soc.*, **120**, 12108 (1998).
12. S. Ronnebeck, J. Carstensen, S. Ottow, and H. Föll, *Electrochem. Solid-State Lett.*, **2**, 126 (1999).
13. V. Lehmann, R. Stengl, and A. Luigart, in Proceedings of the E-MRS Symposium I, Strassbourg, France, June (1999).